Journal of Alloys and Compounds 509 (2011) 9296–9301

Contents lists available at ScienceDirect

Journal of Alloys and Compounds

journal homepage: www.elsevier.com/locate/jallcom

Thermoelectric properties of $Bi_2Se_xTe_{3-x}$ prepared by Bridgman method

N. Keawprak[a,*], S. Lao-ubol[a], C. Eamchotchawalit[a], Z.M. Sun[b]

[a] Thailand Institute of Scientific and Technological Research, Pathum Thani 12120, Thailand
[b] National Institute of Advanced Industrial Science and Technology, Nagoya 463-8560, Japan

ARTICLE INFO

Article history:
Received 2 April 2011
Received in revised form 25 June 2011
Accepted 30 June 2011
Available online 20 July 2011

Keywords:
Bridgman method
Thermoelectric property
$Bi_2Se_xTe_{3-x}$
Thermal conductivity

ABSTRACT

$Bi_2Se_xTe_{3-x}$ crystals with various x values were grown by Bridgman method. The electrical conductivity, σ, was found to decrease with increasing Se content. The highest σ of 1.6×10^5 S m^{-1} at room temperature was reached at $x = 0.12$ with a growth rate of 0.8 mm h^{-1}. The Seebeck coefficient, S, was less dependent on Se content, all with positive values showing p-type characteristics, and the highest S was measured to be 240 μV K^{-1} at $x = 0.24$. The lowest thermal conductivity, κ, was 0.7 W m^{-1} K^{-1} at $x = 0.36$. The electronic part of κ, κ_{el}, showed a decrease with increasing Se content, which implies that the hole concentration as the main carriers was reduced by the addition of Se. The highest dimensionless figure of merit, ZT, at room temperature was 1.2 at $x = 0.36$, which is attributed to the combination of a rather high electrical conductivity and Seebeck coefficient and low thermal conductivity.

1. Introduction

Bi_2Te_3-based alloys have been widely used as thermoelectric cooling and heating materials [1–13]. The Bi_2Te_3–Bi_2Se_3 compounds are well known to have excellent thermoelectric properties for n-type material. Many researchers have studied Bi_2Te_3–Bi_2Se_3 compounds in order to improve their figure of merit Z [4,5]. The Z is a function of the thermoelectric power or Seebeck coefficient (S), electrical conductivity (σ) and thermal conductivity (κ) as given by $Z = S^2\sigma/k$. The n-type $Bi_2(TeSe_3)$ single crystal alloy have been usually used as thermoelectric cooling module due to its high figure of merit. This single crystal alloy shows very high anisotropies on thermoelectric properties, e.g. $\sigma_{11}/\sigma_{33} \approx 4, \kappa_{11}/\kappa_{33} \approx 2$ [6]. Thus, the ingot of single crystal exhibits the most excellent thermoelectric performance along the crystal growth direction in c-plane. Materials grown by a directional solidification method, however, have a disadvantage of poor mechanical properties because the basal planes in this rhombohedral structure are weakly bonded by van der Waals force and easy to cleave. The Bi_2Te_3–Se_2Te_3 single crystals are p-type semiconductors in Bi_2Te_3 rich region [7,8]. The single crystals were grown by vertical zone melting by Sokolov et al. [9] and reported that with increasing Bi_2Se_3 in Bi_2Te_3 at less than 20 mol% Bi_2Se_3, the S showed positive values (p-type conduction) whereas that of higher than 20 mol% Bi_2Se_3 showed negative values (n-type conduction). Kim et al. [10] found that in single crystal, a p–n transition occurred at about 30 mol% Bi_2Se_3 whereas the hot-pressed specimens exhibited n-type conduction for all compositions. In the preliminary study of Bridgman method, it was found that thermoelectric properties change drastically depending on process parameters. In addition, the difference of carrier generation mechanism in $Bi_2Se_xTe_{3-x}$ system by Bridgman method was not clarified. In the present study, we studied the effect of Se content in $Bi_2Se_xTe_{3-x}$ ($x = 0.12$–0.60) by Bridgman method on their thermoelectric properties.

2. Experimental

Powders of Bi (−100 mesh, Aldrich), Se (−200 mesh, Aldrich) and Te (200 mesh, Acros organics), all with purity of >99%, were employed as starting materials. The appropriate amount of powders were weighed for $Bi_2Se_xTe_{3-x}$ ($x = 0.12$–0.60) and charged into a vial with tungsten carbide-balls as milling media under N_2 atmosphere. Ball-to-powder weight ratio was held at 5:1. In order to reach homogeneous mixing of the starting materials as well as to suppress possible losses of low melting point elements during the following process, as a pre-treatment, mechanical alloying was conducted by superimposed rotational movement of grinding balls in the vial at 180 rpm for 48 h using planetary mill Pulverisette 5. X-ray diffraction (Shimadzu, XRD6000) was applied to ascertain the formation of alloy powders. The $Bi_2Se_xTe_{3-x}$ crystal alloy was grown by Bridgman method in a sealed graphite tube (inner dia. 20 mm) with a conical bottom. Powders were melted at 973 K for 7 h before growing the crystals at a rate of 0.8 mm h^{-1} for all compositions. For the composition of $x = 0.12$, the crystal was also grown at another rate of 3.0 mm h^{-1}. The axial temperature gradient was estimated to be 2.4 K mm^{-1} in Bridgman furnace. The grown crystals were about 40 mm in length and 65 g in mass. Specimens were cut from the crystals parallel and perpendicular to the growth direction, which are designated as longitudinal and transverse directions for electrical and thermal measurements, respectively. The specimens with size of 4 mm × 4 mm × 20 mm were used for the measurement of Seebeck coefficient and electrical conductivity using ZEM-2, Ulvac-Riko in a helium atmosphere. The disk specimens with 10 mm in diameter and 1 mm in thickness were measured for thermal conductivity using Laser flash TC-7000, Ulvac-Riko in a vacuum atmosphere. All measurements were conducted from room temperature to 503 K.

* Corresponding author. Tel.: +66 25779439; fax: +66 25779426.
E-mail address: nittaya@tistr.or.th (N. Keawprak).

0925-8388/$ – see front matter © 2011 Elsevier B.V. All rights reserved.
doi:10.1016/j.jallcom.2011.06.116

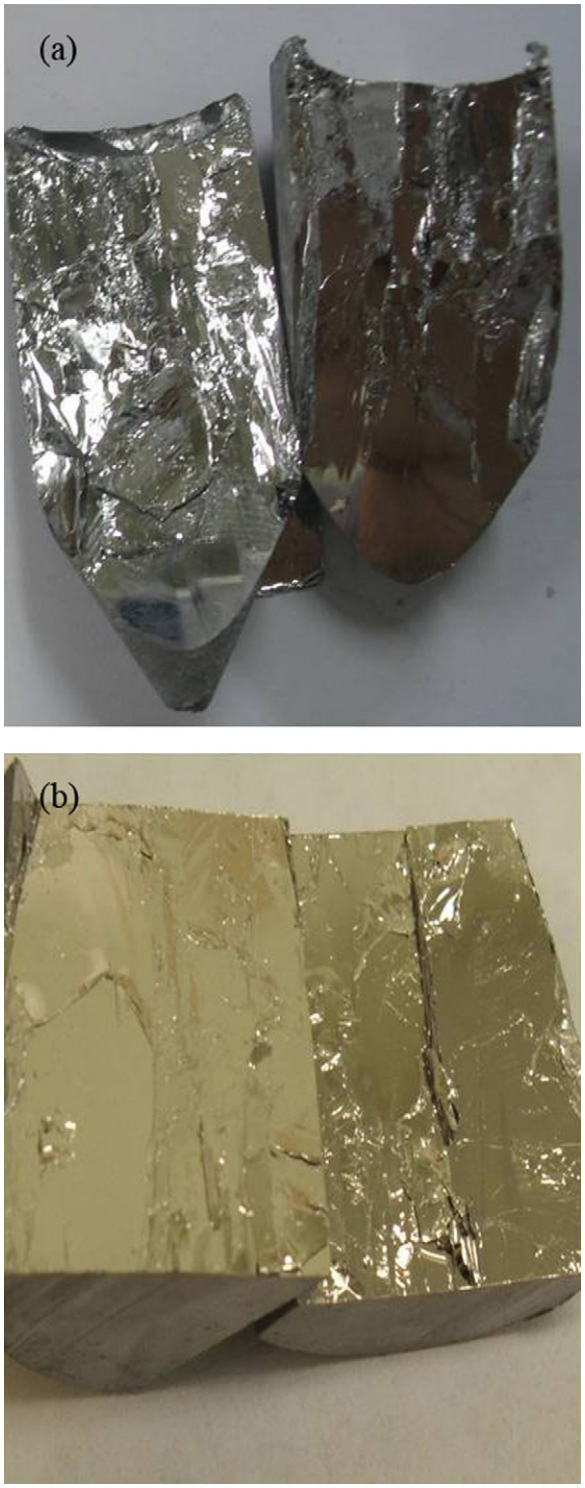

Fig. 1. Fracture appearance of samples $Bi_2Se_{0.12}Te_{2.88}$ grown at a growth speed (a) 3.0 mm h^{-1} and (b) 0.8 mm h^{-1}, respectively.

3. Results and discussion

As an example, the compound of $Bi_2Se_{0.12}Te_{2.88}$ grown at a growth speed 3.0 mm h^{-1} and 0.8 mm h^{-1} are shown in Fig. 1(a) and (b), respectively, which were either cleaved along the plane parallel to the crystal growth direction.

Fig. 2 shows XRD patterns of $Bi_2Se_{0.12}Te_{2.88}$ after mechanical alloying (MA) and crystal growth in Bridgman furnace. The MAed powders were identified to be a single phase of $Bi_2Se_{0.12}Te_{2.88}$ with broad peaks as shown in Fig. 2(a). Compared with the crystal grown at 3.0 mm h^{-1} (Fig. 1(a)), the one grown at 0.8 mm h^{-1} (Fig. 1(b)) was cleaved with a much evener fracture plane parallel to growth direction with its X-ray diffraction pattern shown in Fig. 2(b). The XRD pattern showed planes of (0 0 6), (0 0 1 5), (1 0 1 6) and (0 0 2 1) which indicated that the ingots were not single crystals, but consisted of very coarse grains with the (0 0 *l*) planes aligned approximately parallel to the growth direction. The crystals grown at 3.0 mm h^{-1} and 0.8 mm h^{-1} were cut along the growth axis (longitudinal) as shown in Fig. 2(c) and (d), respectively. The XRD patterns in longitudinal direction of these two crystals were identified to have preferred orientation peaks in (0 0 *l*) planes which were not observed in transverse direction as shown in Fig. 2(e). By comparing the XRD patterns of longitudinal samples as shown in Fig. 2(c) and (d), it is evident that the crystal grown at 0.8 mm h^{-1} shows more preferential orientation degree on *c*-plane than that grown at 3.0 mm h^{-1}.

Table 1
Lattice parameters *a*, *c* and volume of $Bi_2Se_xTe_{3-x}$ crystals at various Se contents.

Specimen	*a* (nm)	*c* (nm)	Volume (nm^3)
$Bi_2Se_{0.12}Te_{2.88}$	0.4373	3.0428	0.5039
$Bi_2Se_{0.24}Te_{2.76}$	0.4368	3.0410	0.5025
$Bi_2Se_{0.36}Te_{2.64}$	0.4349	3.0248	0.4954
$Bi_2Se_{0.48}Te_{2.52}$	0.4338	3.0240	0.4928
$Bi_2Se_{0.60}Te_{2.40}$	0.4328	3.0136	0.4887

In order to identify the phase compositions and to calculate the lattice parameters of the grown ingots, pieces were taken from every ingot and ground to powders for XRD examination. Fig. 3 shows the XRD patterns of such powders of $Bi_2Se_xTe_{3-x}$ at $x = 0.12$, 0.24, 0.36, 0.48 and 0.60, respectively. Single phase of $Bi_2Se_xTe_{3-x}$ was identified in the patterns of $x = 0.12$, 0.24, 0.36. The preferentially stronger reflections on the (0 0 *l*) planes measured in all the powder samples are indicative that the powder particles are flake shaped and readily aligned on the (0 0 *l*) planes when filled into the sample holders. Most peaks shifted to higher angles with increasing Se. Small peaks at 2θ of 17.85°, 26.40° and 35.54° detected in the samples $x = 0.48$ and 0.60 were identified to be (0 0 6), (0 0 9) and (0 0 1 2) planes of Bi_2SeTe_2 phase. This result demonstrates that a small amount of Bi_2SeTe_2 secondary phase was formed in $Bi_2Se_xTe_{3-x}$ at $x \geq 0.48$. The mixture of two-phases also occurred in $Bi_2Se_xTe_{3-x}$ at $x = 0.39$–1.0 as shown in the phase diagram of the Bi_2Te_3–Bi_2Se_3 with zone-melted samples reported by Sokolov et al. [9]. The second phase of Bi_2SeTe_2 also shows preferred orientation in (0 0 *l*) planes. Lattice parameters of $Bi_2Se_xTe_{3-x}$ were calculated from the XRD patterns and summarized in Table 1. Both the values of *a* and *c* decreased with increasing Se concentration. This is easily understood that the substitution of Te atom with smaller Se atoms in Bi_2Te_3 resulted in lattice shrinkage.

Fig. 4(a) shows the morphology of a grown crystal with about 40 mm in length and 20 mm in diameter. Fig. 4(b) and (c) shows the SEM fractographs of grown crystal in transverse direction. The grains were arranged in layered crystallographic structure and the Te(1)–Te(1) layers are bonded by van der Waals force [11]. The grains cleave easily from *c*-planes between Te(1)–Te(1), as revealed in Fig. 4(d) and (e). It is evident that the grains in the ingots grown under Bridgman conditions crystallized preferentially with the basal *c*-planes parallel to the growth direction.

Fig. 5 shows the temperature dependence of electrical conductivity (σ) of $Bi_2Se_xTe_{3-x}$ ($x = 0.12$–0.60) in longitudinal direction. The σ of all specimens decreased with increasing temperature exhibiting metallic conduction. Among the crystals grown at the same rate of 0.8 mm h^{-1}, the σ value of $x = 0.12$ was the highest in the entire testing temperature range, with a value of 1.6×10^5 S m^{-1} at room temperature. It is interesting to note that, when the

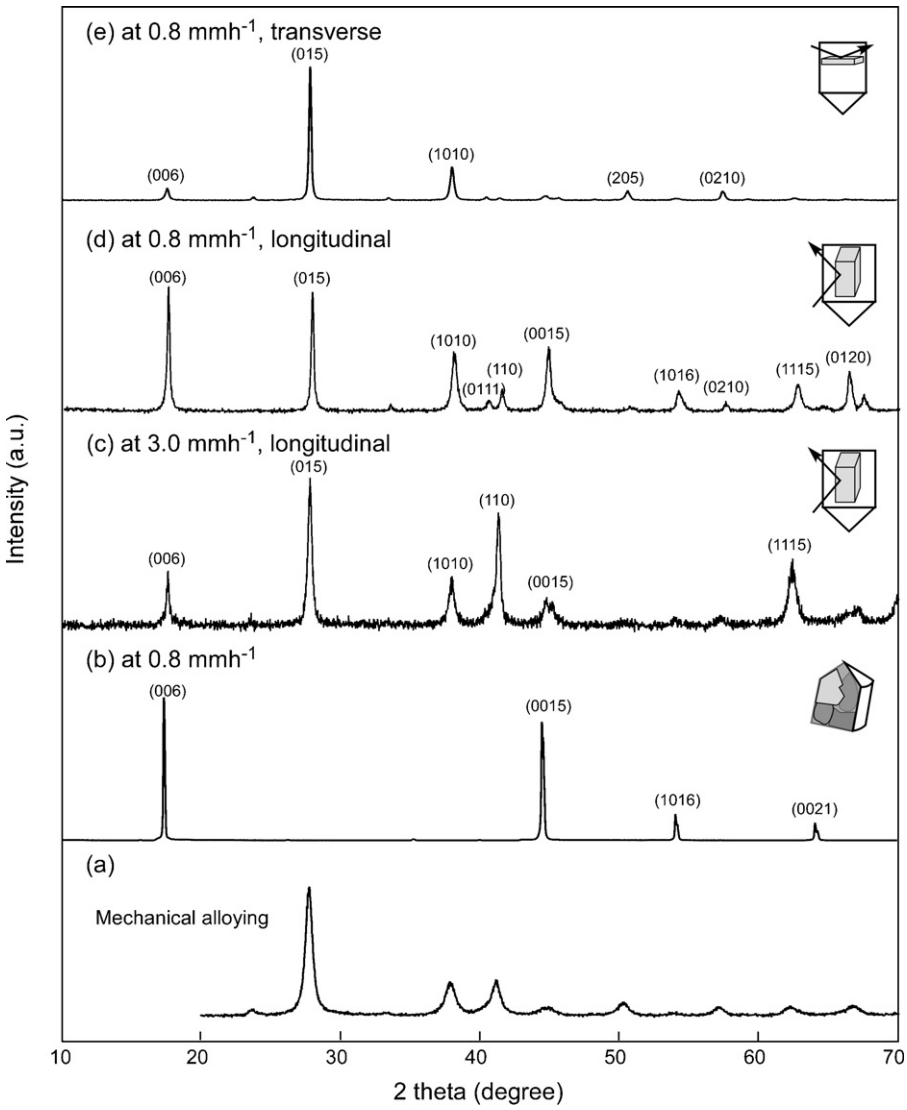

Fig. 2. XRD patterns of $Bi_2Se_{0.12}Te_{2.88}$ compounds: (a) as MAed powders (b) cleaved fracture surface (as shown in Fig. 1(b)) at a growth speed 0.8 mm h^{-1}, the cut and polished sample surface along (c) longitudinal direction at a growth speed 3.0 mm h^{-1}, (d) longitudinal direction and (e) transverse direction at a growth speed 0.8 mm h^{-1}.

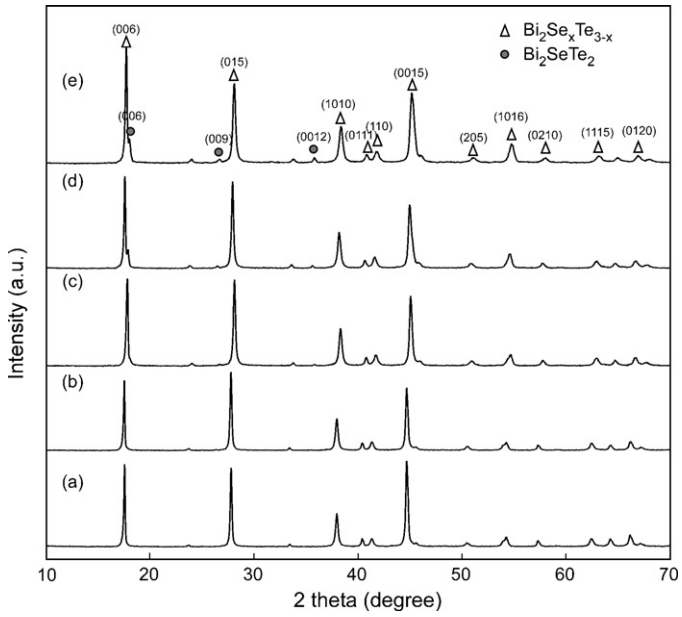

Fig. 3. XRD patterns of pulverized grown $Bi_2Se_xTe_{3-x}$ crystals at (a) $x = 0.12$, (b) $x = 0.24$, (c) $x = 0.36$, (d) $x = 0.48$ and (e) $x = 0.60$, respectively.

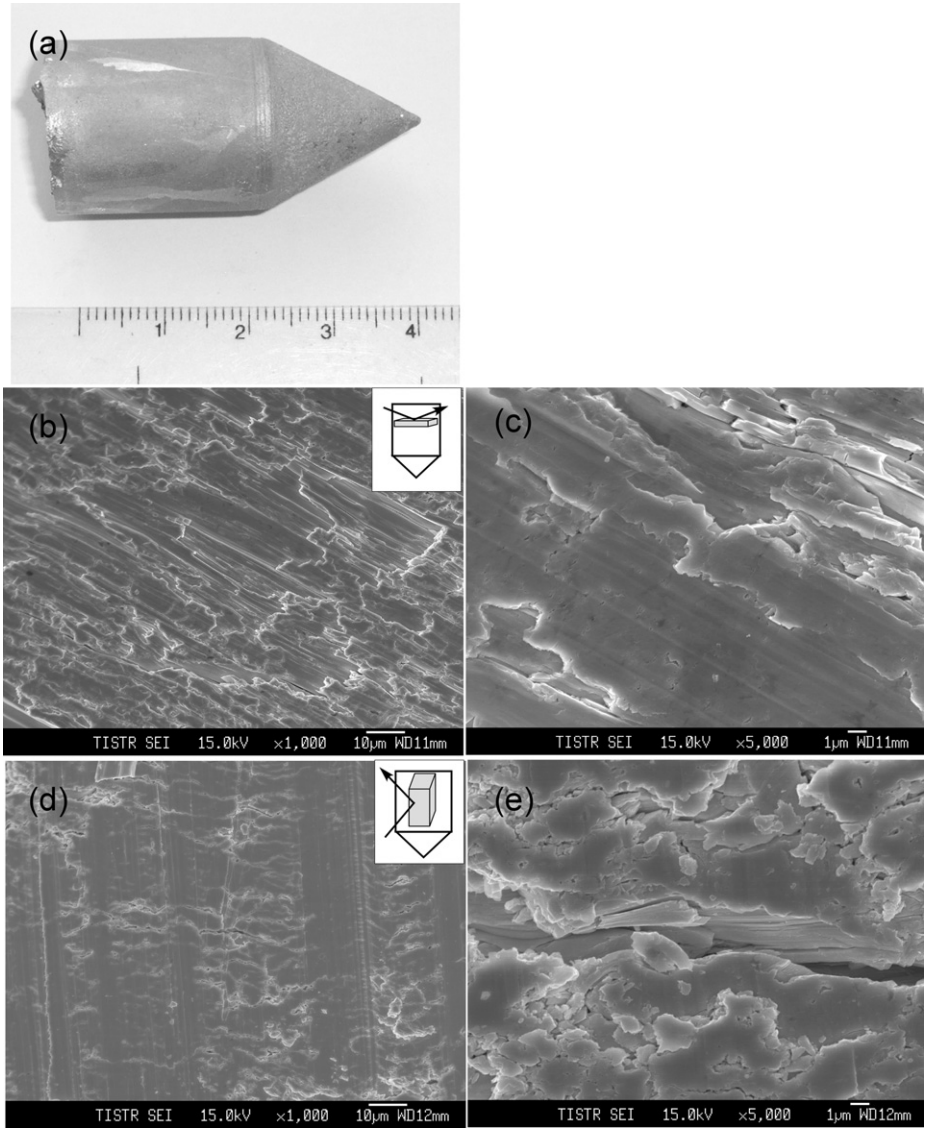

Fig. 4. Optical and scanning electron microscopic images of $Bi_2Se_{0.12}Te_{2.88}$ crystals (a) ingot, ((b) and (c)) perpendicular and ((d) and (e)) parallel to growth axis.

crystal growth rate was increased from 0.8 mm h^{-1} to 3.0 mm h^{-1}, the σ value of the material with $x = 0.12$ was drastically decreased, for almost twofold at room temperature. This is attributed to preferentially orientation of the crystal along basal *c*-planes. The σ in the *c*-plane are 4 times larger than the *c*-axis in Bi_2Te_3-based alloys [6]. The higher σ found in the crystal grown at 0.8 mm h^{-1} was due to the higher oriented texture, as evidenced by the XRD results in Fig. 2.

By comparing the σ values of the samples with various concentrations of Se, as shown in Fig. 5, it is clear that the σ decreased with increasing Se content. The increase in the concentration of atoms of Se incorporated in the lattice leads to an decrease in the hole concentration. This result is due to the nature of point defects present in the crystal when Se atoms are incorporated. The Se atoms are substituted on the Te(2) sites and that bond polarity Bi–Se(2) is smaller than the bond polarity Bi–Te(2) [12]. If the number of Bi–Se(2) bonds increase, then the average bound polarity decreases. According to Horak et al. [13] the formation energy of antisite defect Bi_{Te} is directly proportional to the bond polarlity in the crystal. We can conclude that the concentration of anion vacancies increases with the content of Se atoms [13].

Fig. 6 exhibits the temperature dependence of Seebeck coefficient (S) of $Bi_2Se_xTe_{3-x}$ ($x = 0.12$, 0.24, 0.36, 0.48 and 0.60). The S of all compositions demonstrated positive values showing p-type conduction. The S of all specimens slightly decreased with increasing temperature from room temperature to 400 K and then decreased considerably with increasing temperature. The S was independent of Se content. At room temperature, the highest S was measured to be 240 μV K^{-1} at $x = 0.24$.

Fig. 7 shows the plot of log (σT) versus $1/T$ for all samples. The relationship between log(σT) and $1/T$ is non-linear in the whole temperature range measured. The log(σT) was found to decrease with ($1/T$) the temperature range of 300–400 K, showing metallic conduction that means free holes in conduction band have sufficient energy to move. However, at temperatures above 400 K, the values of log(σT) either remain constant or show an increase with ($1/T$), which implies that small polaron hopping conduction mechanism occurred at high temperature. For hopping mechanism, electrical conductivity can be given as: $\sigma = nea^2(A/T)\exp(-E_h/kT)$, where n, e, a, k, E_h and A are the carrier concentration, electron charge of carrier, intersite distance of hopping, Boltzmann constant,

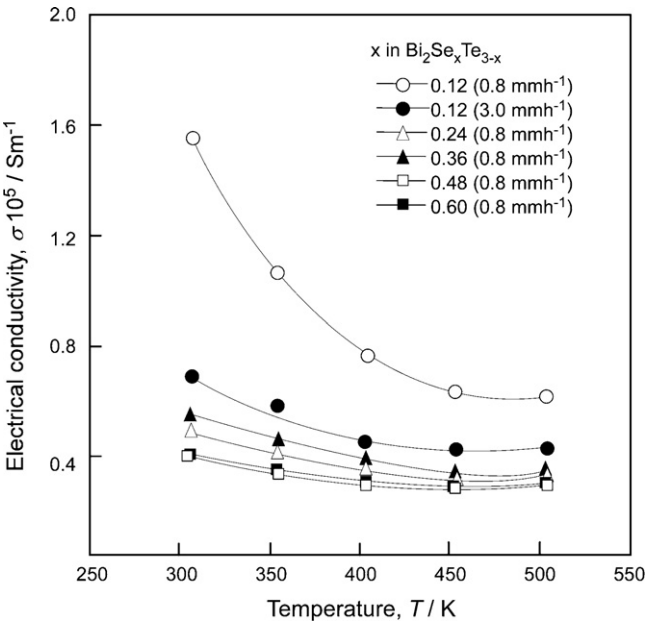

Fig. 5. Temperature dependence of electrical conductivity of $Bi_2Se_xTe_{3-x}$ with various x.

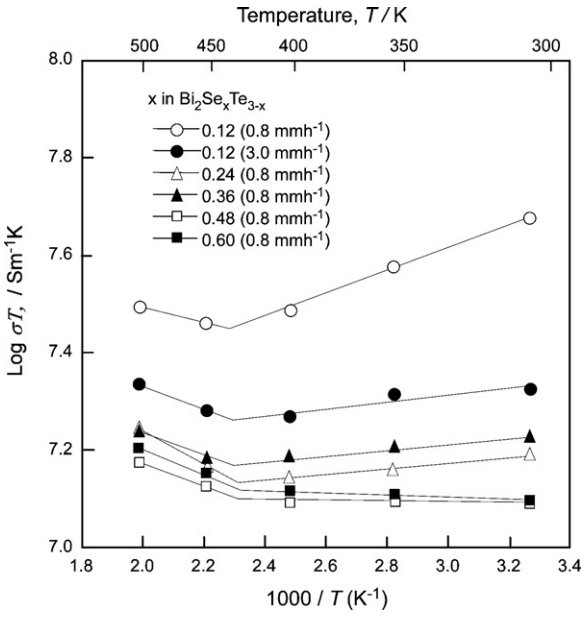

Fig. 7. log(σT) versus 1/T plots of $Bi_2Se_xTe_{3-x}$ at various x.

activation energy, and a pre-exponential term related to the scattering mechanism, respectively. The values of activation energy can be calculated from the slope of plot. For the samples of $x = 0.48$–0.60, the log (σT) slightly increased with increasing temperature implied to be semiconductor behavior. In $Bi_2Se_xTe_{3-x}$ studied herein, it can be concluded that with increasing Se content, hole carrier concentrations decrease and the alloys become hopping conduction.

Fig. 8 exhibits temperature dependence of thermal conductivity (κ) of $Bi_2Se_xTe_{3-x}$ at various Se contents. The κ of $x = 0.12$–0.48 increased with increasing temperature whereas that of $x = 0.60$ decreased with increasing temperature. According to the definition of figure of merit, a low κ value favors the performance of a thermoelectric material. The lowest κ of 0.7 W m^{-1} K^{-1} was found in the sample of $x = 0.36$. The κ can generally be decomposed into two parts, one from the electronic contribution (κ_{el}) and another from the lattice vibration (κ_l). Actually, electronic contributions are the dominant factor in thermal conduction. They are easily excited into the conduction band and the electrons can transfer thermal energy. Thus, the relationship between thermal and electrical conductivity can be expressed as $k_{el}/(\sigma T) = L$. This is called the Wiedeman–Franz relationship, where L is the Lorentz constant. So the lattice contribution can be obtained by $k_l = k_{tot} - k_{el}$. The composition dependence of κ_{tot} and κ_{el} are shown in Fig. 9. The κ_{tot} decreased with increasing Se content from 2.2 to 0.7 W m^{-1} K^{-1} at $x = 0.12$–0.36 and then increased sharply to 2.5–3.2 W m^{-1} K^{-1} at $x = 0.60$ and 0.48, respectively. The plot between κ_{el} and composition shows that κ_{el} decreased with increasing Se content. It can be attributed to hole carrier concentration reduced when Se content increased. The thermal conductivity at $x = 0.12$–0.36 come from the electronic contribution around 40–60% whereas that at $x = 0.48$ and 0.60 come from the lattice vibration around 90%.

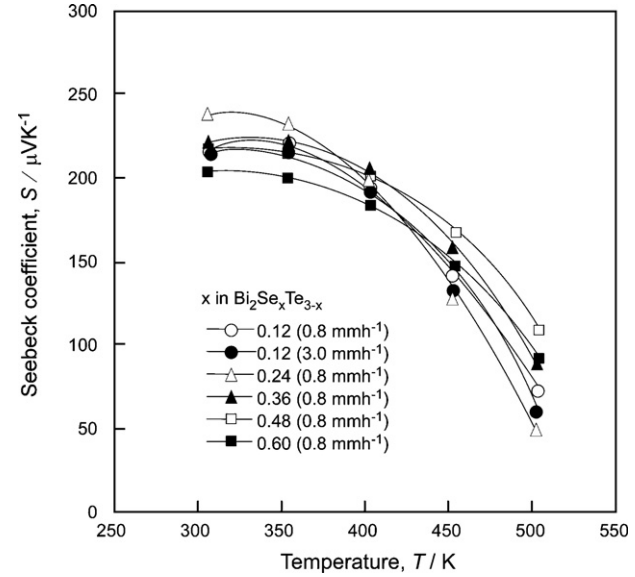

Fig. 6. Temperature dependence of Seebeck coefficient of $Bi_2Se_xTe_{3-x}$ at various x prepared by hot pressing method.

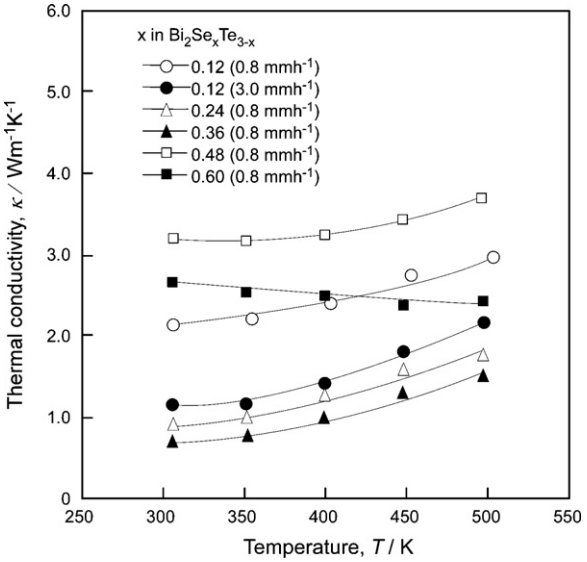

Fig. 8. Temperature dependence of thermal conductivity of $Bi_2Se_xTe_{3-x}$ at various x.

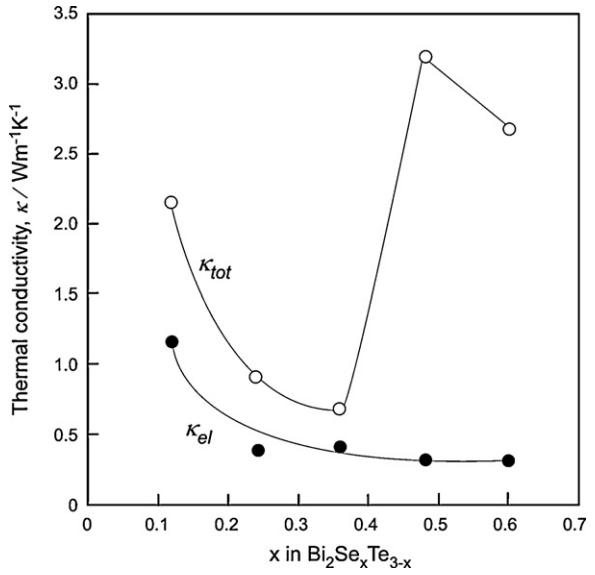

Fig. 9. The relationship between Se content at various x and κ_{tot} and k_{el} at room temperature.

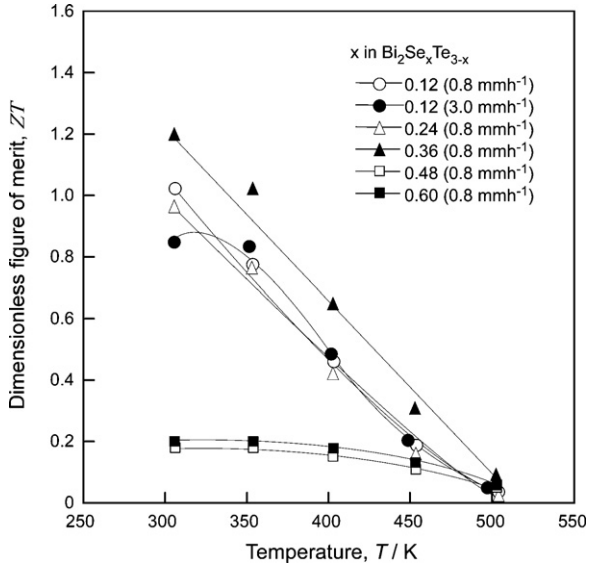

Fig. 10. Temperature dependence of ZT of $Bi_2Se_xTe_{3-x}$ at various x.

Fig. 10 shows temperature dependence of dimensionless figure of merit (ZT). The quality of thermoelectric materials was described by a ZT which is calculated from the equation of $ZT = \alpha^2\sigma T/k$. The ZT of all specimens decreased with increasing temperature. The maximum value of ZT was 1.2 at $x = 0.36$ and at room temperature because of combination of a rather high electrical conductivity and Seebeck coefficient and low thermal conductivity.

4. Conclusions

$Bi_2Se_xTe_{3-x}$ compounds with various x values were prepared by Bridgman method. The electrical conductivity was found to decrease with increasing Se content. All samples show p-type conduction and metallic behavior. The Seebeck coefficients of the alloys were found to be independent of Se content. The lowest thermal conductivity, κ, was at $x = 0.36$ around 0.7 $W\,m^{-1}\,K^{-1}$. The κ_{el} decreased with increasing Se content that implied that hole carrier concentration reduced when Se content was added. The highest of dimensionless figure of merit (ZT) was measure to be 1.2 at $x = 0.36$ and at room temperature due to the combination of a rather high electrical conductivity and Seebeck coefficient and low thermal conductivity.

Acknowledgment

This work was financially supported by National Metal and Material Technology Center (MTEC) under Grant No. MT-B-S1-END-37-048-G.

References

[1] N. Keawprak, Z.M. Sun, H. Hashimoto, M.W. Barsoum, J. Alloys Compd. 397 (2005) 236.
[2] Z.M. Sun, H. Hashimoto, N. Keawprak, A.B. Ma, L.F. Li, M.W. Barsoum, J. Mater. Res. 20 (2005) 895.
[3] C. Chen, D.-W. Liu, B.-P. Zhang, J.-F. Li, J. Electron. Mater. 40 (2011) 942–947.
[4] S.A. Ahmed, E.M.M. Ibrahim, S.A. Saleh, Appl. Phys. A: Mater. Sci. Process. 85 (2) (2006) 177.
[5] J. Choi, H.W. Lee, B.S. Kim, H. Park, S. Choi, S.C. Hong, S. Cho, J. Magn. Mater. 304 (1) (2006) e164.
[6] D.M. Rowe, CRC Handbook of Thermoelectrics, CRC Press, Boca Raton, 1995, p. 211.
[7] D.L. Greenaway, G. Harbeke, J. Phys. Chem. Solids 26 (1965) 1585.
[8] D.B. Hyun, H.P. Ha, J.D. Shim, Proc. XI International Conf. Thermoelectrics, Arlington, TX, 1992, p. 266.
[9] O.B. Sokolov, S.Ya. Skipidarov, N.I. Duvankov, G.G. Shabunina, J. Cryst. Growth 262 (2004) 442.
[10] H.C. Kim, S.K. Lee, T.S. Oh, D.B. Hyun, 17th International Conference on Thermoelectrics, 1998, p. 125.
[11] Z. Stary, J. Horak, M. Stolzer, J. Phys. Chem. Solids 49 (1988) 29.
[12] R. Ionescu, J. Iaklovszky, N. Nistor, A. Chiculita, Phys. Status Solidi A 27 (1975) 27.
[13] J. Horak, Z. Stary, J. Votinsky, Philos. Mag. B 55 (1994) 327.